

# Al-Mg Alloys prepared by Mechanically Alloying Reinforced with Carbon Nanotubes and their Corrosion Behavior in Bioethanol

*E.J. Moreno Carpintero<sup>1</sup>, I. Santos Ramos<sup>1</sup>, G. Rosas<sup>1</sup>, M. A. Espinosa Medina<sup>2</sup>,  
E. Sarmiento-Bustos<sup>3</sup>, R. Lopez-Sesenes<sup>4</sup>, J.G. Gonzalez-Rodriguez<sup>4,\*</sup>*

<sup>1</sup> Instituto de Investigación en Metalurgia y Materiales, UMSNH, Av. Fco. J. Mujica S/N C.U. Morelia Mich. 58230, México.

<sup>2</sup> Facultad de Ing. Mecanica, UMSNH, Av. Fco. J. Mujica S/N C.U. Morelia Mich. 58230, México.

<sup>3</sup> Universidad Tecnológica Emiliano Zapata, Zapata, Morelos, Mexico

<sup>4</sup> Universidad Autonoma del Estado de Morelos, CIICAP, Av. Universidad 1001, Col. Chamilpa, Cuernavaca, Mor., Mexico

\*E-mail: [ggonzalez@uaem.mx](mailto:ggonzalez@uaem.mx)

*Received: 7 December 2019 / Accepted: 29 January 2020 / Published: 10 March 2020*

---

Two different Al-Mg alloys containing 4 and 6 wt.% Mg were mechanically produced and reinforced with 0.05 wt.% Carbon nanotubes (CNT) and corroded in fuel grade bioethanol (FGB). Employed techniques for the corrosion tests included potentiodynamic polarization curves, linear polarization resistance and electrochemical impedance spectroscopy measurements. Results have shown that there was no evidence of the formation of a passive layer on top of the specimens. Corrosion rate increased with the increase in the Mg contents and the addition of CNTs. Specimens exhibited a type of localized corrosion similar to pits, which increased in number, size and depth with the addition of Mg and CNTs in the alloys.

---

**Keywords:** Al-Mg composites; bioethanol; corrosion.

## 1. INTRODUCTION

Now days, biofuels represent a solution for the pollution that fossil fuels produce and an alternative to satisfy the increasing demand of energy. Automotive fuel has met the challenge to reduce the use of fossil fuels and to improve their efficiency. Bioethanol is a promising candidate as an alternative source of energy for automotive applications [1-4]. In order to decrease environmental pollution due to the emissions from car engines, bioethanol has been as a promising candidate to be used as an alternative source of energy instead of using traditional oil. Bioethanol can be mixed or blended

with gasoline in any percentage although commercially is only used between 10 to 30 vol. % of ethanol, the so called E10-E30, helping to reduce fuel costs by approximately 3% [5-7]. Moreover, bio-ethanol blended gasoline fuels can reduce the fuel cost of automotive to approximately 1–3% with increasing ethanol content by E10–E30 (ethanol vol. %) compared to regular unleaded gasoline [5–7].

The corrosion performance of automotive metallic components depends greatly on the use of bioethanol as fuel due to the presence of water and the formation of aggressive compounds. Most of the companies that fabricate cars in the world have made the fuel system and engines in such a way that they run at any ethanol content even up to E100 fuel [8]. The components of the fuel system are made from materials compatible with ethanol, such as stainless steel or polymer. However, commercial cars used mixtures or blends of bioethanol and gasoline where the fuel system and engine are composed of light metal components, particularly aluminum alloys. It is a very well known fact that aluminum-base alloys can corrode in the fuel mixture, resulting in a deterioration of the durability and safety of vehicles. On the other side, fuel grade ethanol (FGE) can be used as substitute of gasoline, and contains H<sub>2</sub>O, methanol, chloride ion and organic compounds (e.g. acetic acid) as impurities, and it can be produced from a variety of feedstocks such as corn and sugar cane. FGE is widely used in mixture with gasoline in the United States and other countries. The presence of the above mentioned impurities in FGE increase the risk of different types of corrosion such as uniform, pitting or stress corrosion cracking for the metals in contact with this type of fuel [9].

Aluminum and its alloys are widely used for automotive components which are in contact with FGE, and, thus, susceptible of corrosion. Aluminum alloys have been reinforced with ceramics becoming in to aluminum matrix composites (AMCs) which have found many applications due to their high specific strength, lightweight, good wear, corrosion resistance and other features beneficial to superior performance [10, 11]. Many reinforcements such as SiC, Al<sub>2</sub>O<sub>3</sub>, TiC, ashes, graphite, etc. have been used by different authors [12-16] to fabricate AMCs. Carbon nanotubes (CNTs) have been used as AMCs reinforcement since they improve not only their friction and wear properties [17], their hardness and compressive strength [18, 19] and in general, an improvement on their mechanical properties [20, 21] but affect their corrosion properties also [22-24]. Thus, the goal of this research work is to evaluate the corrosion properties of an Al-Mg alloy reinforced with Carbon nanotubes (CNTs) in a FGE environment.

## 2. EXPERIMENTAL PROCEDURE

The synthesis of the CNTs is given in detail elsewhere [25] but briefly a mixture of ferrocene and toluene was used by the spray pyrolysis method in a quartz crucible, at 850 °C during 60 minutes. The use of ferrocene left some Fe particles as contaminant. Al-Mg, with 4 and 6 wt. % Mg were mechanically alloyed by using micrometric powders from Sigma Aldrich and using a Restch PM-100 equipment. Al-Mg powder alloys were mixed with 0.05 wt. % CNTs at a uniaxial pressure of 516 MPa. Thus, in addition to the Al-Mg alloys containing 4 and 6% of Mg and 0.5 CNTs, the respective alloys without reinforcement as well as pure Al were used.

Corrosion tests were performed in a three electrode glass cell using as electrolyte a solution consisting of fuel grade ethanol (FGE) consisting of ethanol+0.5 vol. % methanol+0.5 H<sub>2</sub>O+10 mg/L NaCl+56 mg/L acetic acid, using a Ag/AgCl and a graphite rod as reference and auxiliary electrodes respectively. Used electrochemical techniques included potentiodynamic polarization curves, linear polarization resistance (LPR) and electrochemical impedance spectroscopy (EIS) measurements. Before starting, the free corrosion potential value,  $E_{\text{corr}}$ , was left to reach a steady state value. Once it was stable, scanning started in a potential value of 750 mV more cathodic than the  $E_{\text{corr}}$  value and ended 750 mV more anodic at a scan rate of 1 mV/s. Tafel extrapolation was used to calculate the corrosion current density values,  $I_{\text{corr}}$ . For the LPR tests, a potential of  $\pm 15$  mV around the  $E_{\text{corr}}$  value was applied at a scan rate of 1 mV/s every 60 minutes during 24 hours. Finally, for the EIS measurements, a sinusoidal signal with an amplitude of  $\pm 15$  mV peak-to-peak was applied at the  $E_{\text{corr}}$  value. Corroded specimens were analysed in a low vacuum Scanning electronic microscope (SEM) whereas chemical micro analysis was performed by using an Energy dispersive spectroscopy (EDS) analyser attached to it.

### 3. RESULTS AND DISCUSSION

The effect of Mg and CNTs addition to Al on the change in the open circuit potential value, OCP, with time in FGE is given in Fig. 1.

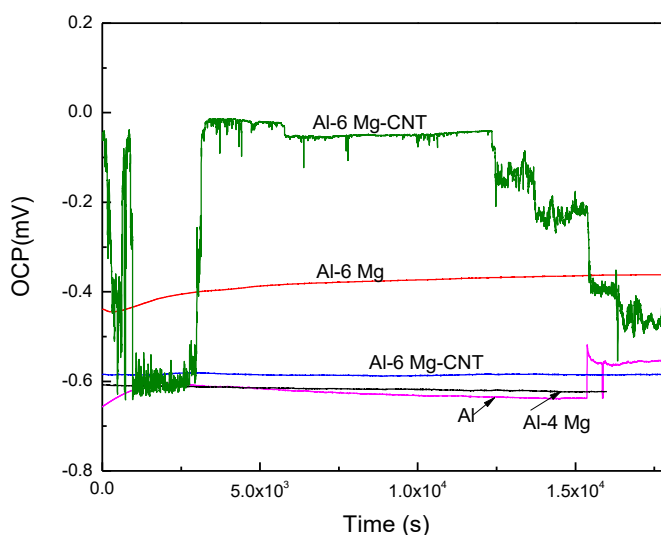


**Figure 1.** Change in the OCP value with time for the different Al-base composites in FGE.

It can be seen that the OCP value for pure Al, Al-4Mg and Al-4Mg-CNT were virtually the same, around -600 mV, and remained very stable during the testing time as reported elsewhere [22-24]. These alloys exhibited the most active OCP values, and thus, the highest susceptibility to be corroded. On the other hand, Al-6Mg and Al-6Mg-CNT alloys showed nobler OCP values, with a decreased susceptibility to be corroded, however, the OCP value for the unreinforced alloy had an erratic behavior, maybe due

to an oxide formation and its breakdown. Thus, it seem that the addition of CNT to both Al-Mg alloys made the OCP value to shift in to nobler values. Alaneme et al. [22] evaluated the corrosion behavior of Al–Mg–Si alloy reinforced with Al<sub>2</sub>O<sub>3</sub> particles and rice husk ash in 3.5% NaCl solution. As compared to the alloy containing only Al<sub>2</sub>O<sub>3</sub> particles, the addition of rice husk ash shifted the OCP value in to nobler values regardless of its amount (2, 3 or 4 wt. %). The higher the amount of rice hush ash, the nobler the OCP value was. However, in all cases, the OCP value had an erratic behavior as time elapsed, attributing this behavior to the formation and breakdown of an Al<sub>2</sub>O<sub>3</sub> layer on top of the alloy [22].

Polarization curves for Al-Mg alloys with and without CNTs reinforcement as well as that for pure Al in FGE are shown in Fig. 2 whereas their electrochemical parameters are given in table 1.

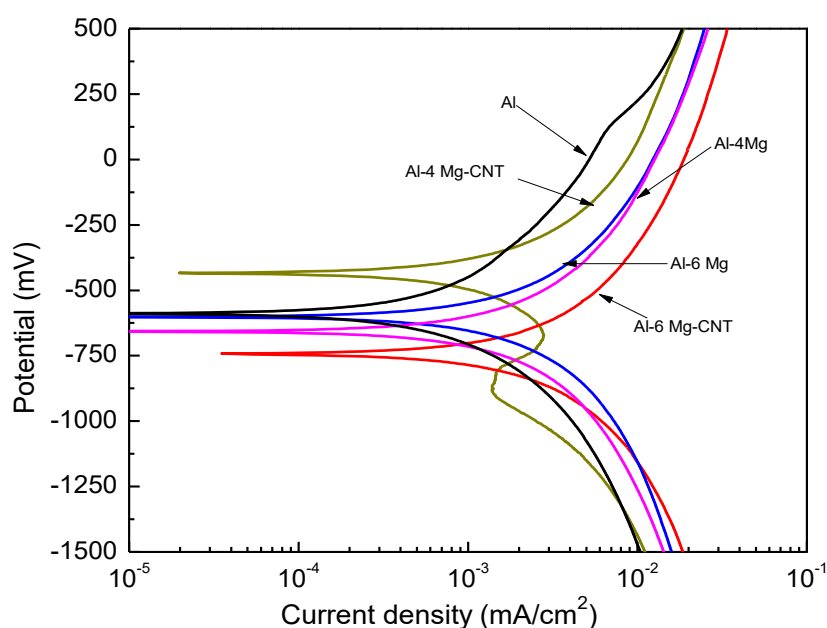


**Figure 2.** Potentiodynamic polarization curves for the different Al-base composites in FGE.

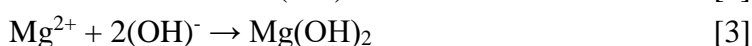
**Table 1.** Electrochemical parameters obtained from the polarization curves for the Al-base composites in FGE.

Alloy	E <sub>corr</sub> (mV)	I <sub>corr</sub> (mA/cm <sup>2</sup> )	β <sub>a</sub> (mV/dec)	β <sub>c</sub> (mV/dec)
Al	-590	3.5 x 10 <sup>-4</sup>	300	550
Al-4Mg	-670	2.1 x 10 <sup>-3</sup>	270	500
Al-4Mg-CNT	-440	5.5 x 10 <sup>-3</sup>	260	480
Al-6Mg	-605	2.8 x 10 <sup>-3</sup>	270	430
Al-6Mg-CNT	-740	8.8 x 10 <sup>-3</sup>	260	550

It can be seen that all the curves for the different alloys, regardless of the Mg content or the presence of CNT as reinforcement, displayed an active behavior, without evidence of a passive layer. The curve for pure Al, as it can be seen in table 1, showed one of the most active E<sub>corr</sub> values and the

lowest  $I_{\text{corr}}$  values. Both anodic and cathodic Tafel slopes were exhibited the highest values for base Al alloy also. It has been shown that the corrosion of pure Al can be dissolved in ethanol following a chemical reaction producing an organic compound, aluminum alkoxide,  $\text{Al}(\text{C}_2\text{H}_5\text{O})_3$ , which dissolves in the electrolyte, therefore the metal is no longer protected [26-28] and the curve displays an active behavior only, with the formation of a passive, protective layer. The noblest  $E_{\text{corr}}$  values were exhibited by the alloys containing 6 Mg with or without the addition of CNTs. It can be seen that the addition of Mg increase the  $I_{\text{corr}}$  value, the higher the Mg contents, the higher the  $I_{\text{corr}}$  value. In both alloys containing CNTs as reinforcement, it is clear that their incorporation was detrimental, since an increase in the  $I_{\text{corr}}$  values was obtained. Alaneme et al. [22] evaluated the corrosion behavior of Al–Mg–Si alloy reinforced with  $\text{Al}_2\text{O}_3$  particles and rice husk ash in 3.5% NaCl solution and found that the lowest  $I_{\text{corr}}$  value was for the alloys without rice husk ash as reinforcement and the corrosion rate increased with its contents. Similarly, Fukuda et al. evaluated the effect of adding 0.89 and 2.66 vol. % CNTs to an Al-Mg alloy, namely AZ31B Mg, on its corrosion behaviour in 3.5% NaCl solution. Polarization curves showed a passive zone for the unreinforced alloy, but the addition of CNTs broke the passive zone, shifted the  $E_{\text{corr}}$  value in to the noble direction for nearly 500 mV and increased the  $I_{\text{corr}}$  value for more than one order of magnitude [29]. In a similar way, Aung et al. [30] evaluated the corrosion resistance of pure Mg reinforced with 0.3 and 1.3 wt. % CNTs in 3.5% NaCl solutions. Polarization curves exhibited an increment in the  $I_{\text{corr}}$  value and a shift if the  $E_{\text{corr}}$  value towards nobler values as the CNTs contents increased. The formation of micro galvanic cells between CNTs, which acted as cathodes, and the matrix, i.e. Mg, was the explanation for such an increment of the Mg corrosion rate as measured in terms of  $I_{\text{corr}}$ . In addition to the existence of CNTs as cathodes, there was also the existence of Fe particles due to the use of ferrocene as catalyst [25], which can act as cathodes. Thus, it seems that the formation of micro galvanic cells with the matrix and the reinforcement CNTs as well as Fe particles is the reason of the increment in the corrosion current density as compared to the alloys without reinforcement.

On the other side, the addition of Mg in to the alloy increases the corrosion current density due to the fact that, in presence of water, Mg dissolves rapidly according to:



Thus, when Mg dissolves, OH ions are released and, thus, increasing the solution pH, and it is very well known that Al decreases its corrosion resistance in alkaline solutions. The more the Mg contents in to the alloy, the higher the solution pH is expected.

Polarization curves are a kind of instant picture of the corrosion processes taking place on a metal surface when exposed to a corrosive environment. Linear polarization measurements, LPR are longer time exposure experiments which will provide us more precise information about these processes. The change in the polarization resistance value,  $R_p$ , for the different composites as a function of time in FGE is shown in Fig. 3. Similar values for  $R_p$  have been reported by Yoo et al. [26] for the corrosion of pure Al in ethanol-gasoline blends. In Fig. 3 it is clear that the highest corrosion resistance, i.e. the highest  $R_p$  value, was for pure Al and the addition of Mg decreased this value, the higher the Mg contents the lower the  $R_p$  value was. On the other hand, the addition CNTs reinforcement decreased the  $R_p$  value also, i.e.

the addition of CNTs as reinforcement particles seems to increase the composite corrosion rate like the reported results in NaCl solutions [22-24, 30].

EIS data in the Nyquist and Bode formats for the different composites in FGE are given in Fig. 4. It can be seen that Nyquist diagrams display two semicircles, one at high and intermediate frequency values, and a second one at lower frequency values as reported in previous research works for Al in ethanol-containing environments [26-28]. The high and intermediate frequency semicircle is related with the interfacial reactions occurring between the metal and the electrolyte, i.e. the double electrochemical layer, whereas the second, low frequency semicircle is related to the interfacial reactions taking place at the corrosion products film.

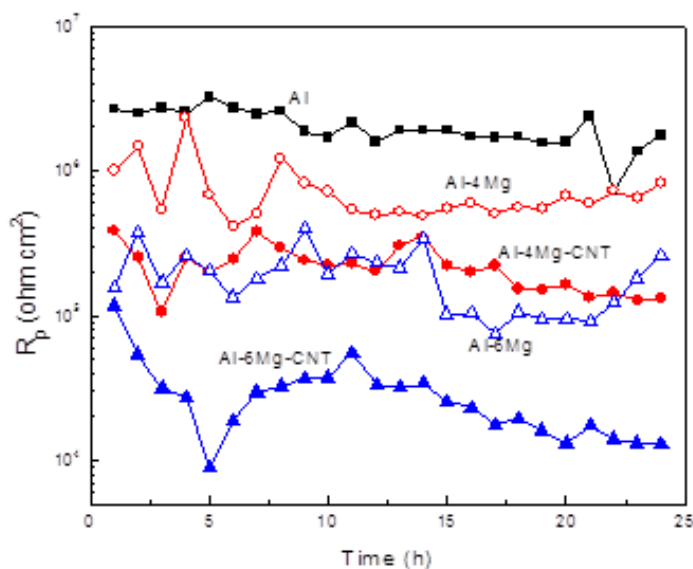


**Figure 3.** Change in the linear polarization resistance value,  $R_p$ , with time for the different Al-base composites in FGE.

EIS data have been simulated by using electric circuit given in Fig. 5 where two time constants were used due to the presence of two semicircles in the Nyquist diagrams. In this figure,  $R_s$  is the solution or electrolyte resistance,  $R_{ct}$  and  $C_{dl}$  (charge transfer resistance and double layer capacitance respectively) are the resistance and capacitance between the metal and the electrolyte, whereas  $R_f$  and  $C_f$  are the resistance and capacitance of the corrosion products film respectively. To take in to account the fact the data in Nyquist diagrams shown in Fig. 4 are depressed and exhibit some dispersion due to heterogeneities on to the metal surface such as surface roughness due to metal dissolution, ideal capacitances have been replaced by a Constant phase element, CPE, in Fig. 5. The impedance of the CPE,  $Z_{CPE}$  is given by [31]:

$$Z_{CPE} = 1/[Y_0(i\omega)^n] \tag{4}$$

where  $Y_0$  is the admittance,  $i = -1^{1/2}$ ,  $\omega$  the angular frequency and  $n$  a physical parameter which gives interphase properties of the working electrode such as roughness, inhibitor adsorption, etc. Parameters used to fit EIS results by using circuits given in Fig. 5 are shown in table 2.

**Table 2.** Parameters used to fit the EIS data for the Al-base composites in FGE.

Alloy	$R_s$ (kohm cm <sup>2</sup> )	$R_{ct}$ (Kohm cm <sup>2</sup> )	$CPE_{dl}$ ( $\mu S s^n/cm^2$ )	$n_{dl}$	$R_f$ (Kohm cm <sup>2</sup> )	$CPE_f$ ( $\mu S s^n/cm^2$ )	$n_f$
Al-	20.1	31.7	$8.7 \times 10^{-10}$	0.9	18.1	$2.7 \times 10^{-12}$	0.9
Al-4Mg	18.2	24.5	$4.5 \times 10^{-13}$	0.8	13.2	$7.3 \times 10^{-12}$	0.8
Al-4Mg-CNT	20.7	20.5	$9.3 \times 10^{-13}$	0.8	10.1	$9.2 \times 10^{-11}$	0.8
Al-6Mg	20.7	19.5	$4.8 \times 10^{-12}$	0.7	11.1	$2.7 \times 10^{-10}$	0.7
Al-6 Mg-CNT	20.6	15.5	$8.1 \times 10^{-12}$	0.7	8.1	$8.2 \times 10^{-10}$	0.7

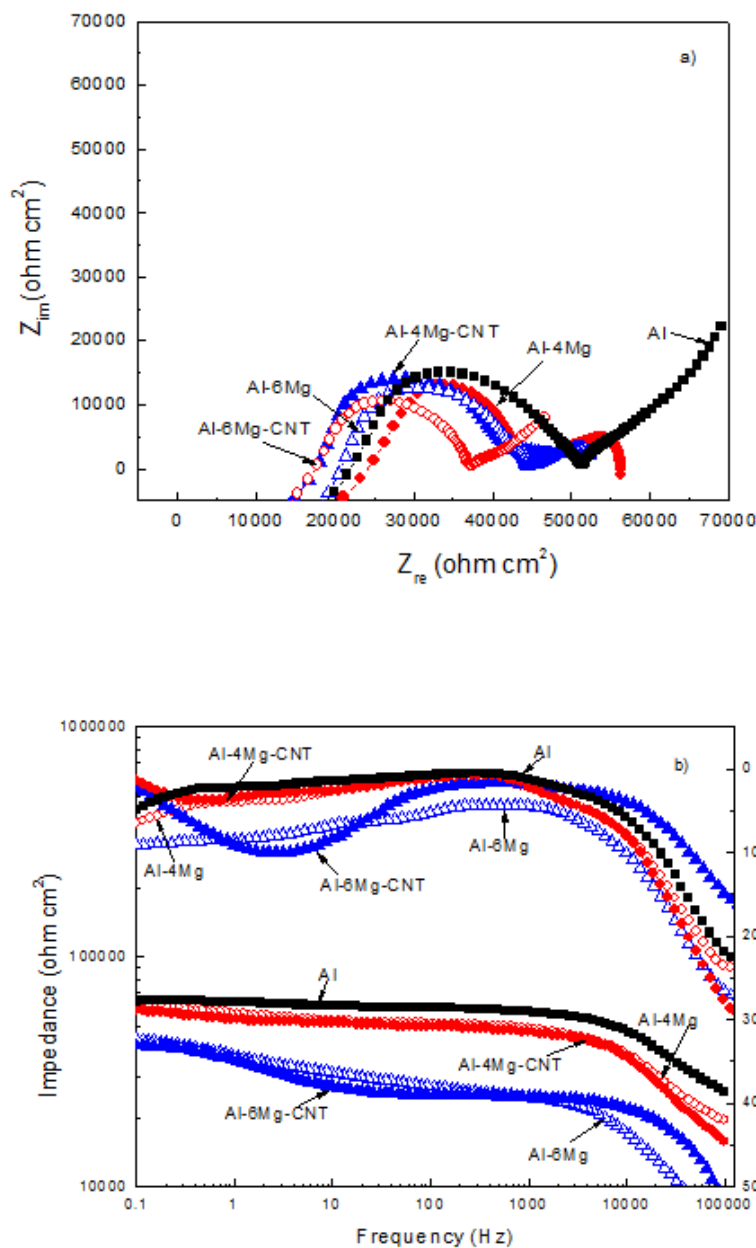


**Figure 4.** EIS data in the a) Nyquist and b) Bode formats for the different Al-base composites in FGE.

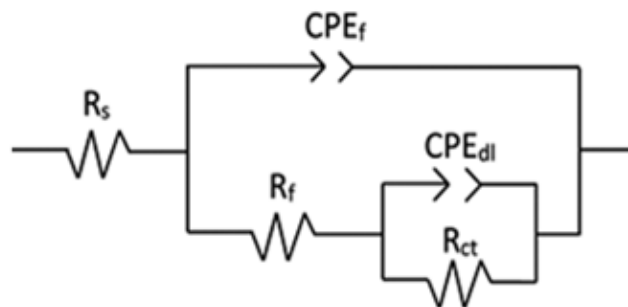


**Figure 5.** Electric circuits used to simulate EIS data for the different Al-base composites in FGE.

It is clear from data given in table 2 that the corrosion resistance of aluminum composites depends upon both, the corrosion resistance of the metal itself, given by the properties of the metal through the double electrochemical layer, i.e.  $R_{ct}$  and  $CPE_{dl}$ , and the properties of the formed protective corrosion products, i.e.  $R_f$  and  $CPE_f$ . The first important fact to note is the high solution resistance values given by  $R_s$ , due to the fact that ethanol is very resistive solution. In order for corrosion to take place, a lower solution resistance is necessary, and the explanation of the corrosion in ethanol containing solutions the presence of water is necessary [32, 33], which might come as sub-product during the ethanol oxidation or as an impurity during storage or during handling [34]. The highest  $R_{ct}$  and lowest  $CPE_{dl}$  values were for pure Al followed by the Al-4Mg alloy with or without CNTs, whereas the lowest  $R_{ct}$  and highest  $CPE_{dl}$  values were for the Al-6 Mg with and without CNTs as reinforcement. On the other hand, the highest  $R_f$  value was also for pure Al and Al-4Mg alloys, whereas the lowest values were for Al-6Mg alloys, explaining why pure Al and Al-6Mg alloys exhibited the lowest  $I_{corr}$  values and why Al-9Mg alloys showed the highest dissolution rates, table 1. An  $n_{dl}$  value close to the unit indicates a very low surface roughness, whereas a value close to 0.5 indicates a high surface roughness. Thus, the lowest  $n_{dl}$  value was for pure Al due a high dissolution rate producing a high surface roughness. On the contrary, the highest  $n_{dl}$  value was for Al-4Mg alloy due to a low dissolution rate and, thus, a low surface roughness. Thus, generally speaking the increment of Mg contents and the presence of CNTs increases the corrosion or dissolution rate.

Micrographs of corroded surfaces in FGE are given in Fig. 6. Pure Al, Fig. 6 a, showed a localized type of corrosion similar to pits, but these were very shallow, as a result of micro galvanic cells between CNTs and Fe particles, which behaved as cathodes, and the Al matrix, which behaved as an active anode. When 4 % Mg was added to Al, Fig. 6 b, the number of pits increased and they were deeper than those found in pure Al, indicating why this alloy exhibited a higher corrosion rate than that for pure Al according to Fig. 2.

Finally, when the CNTs were added to the Al-4 Mg alloy, Fig. 6 c, the number of pits decreased but increased in size and depth, indicating the detrimental effect of the addition of CNTs to the alloy in the corrosion rate as evidenced by data in Fig. 2 and table 1. In none of the observed specimens there was evidence of a passive, protective layer; instead, the corrosion products found, were found in discrete way, without forming a continuous layer, like those shown in Fig. 6 c, which had a chemical composition as given in Fig. 7 in the different composites. EDS spectrum shown in Fig. 7 indicates the

presence of C, O, Al and Mg, and it represents a typical chemical composition of all the corrosion products found.

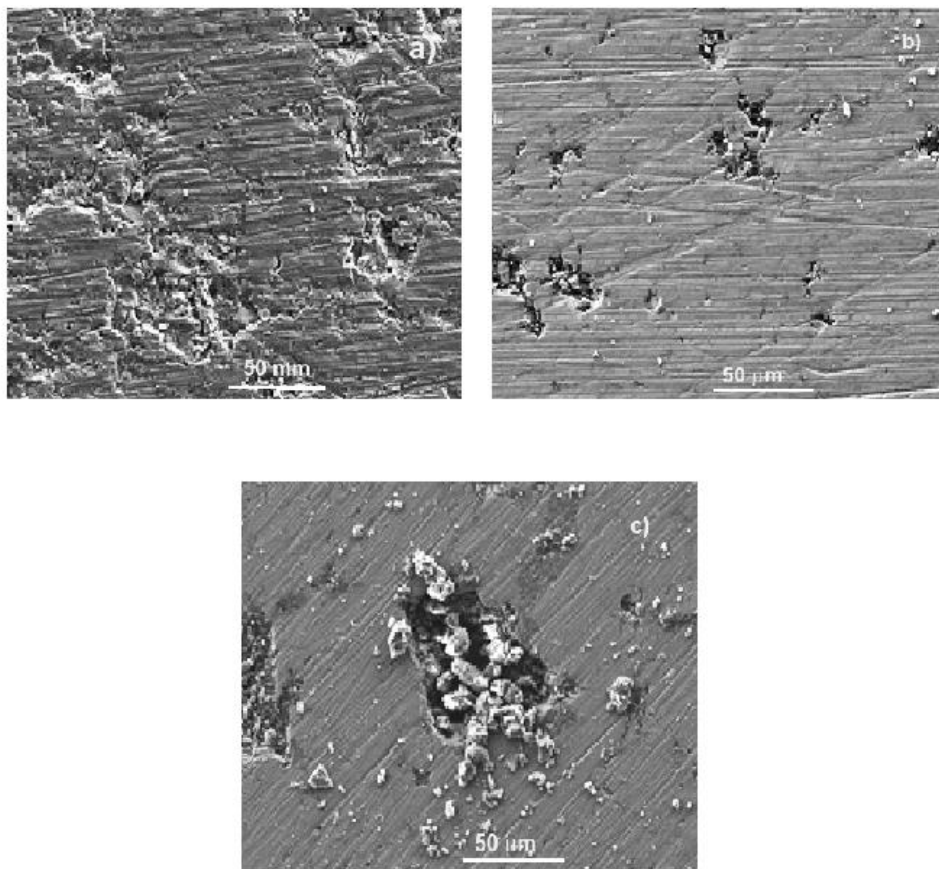


Figure 6. SEM micrographs of a) Al, b) Al-4Mg and c) Al-4Mg-CNT composites corroded in FGE.

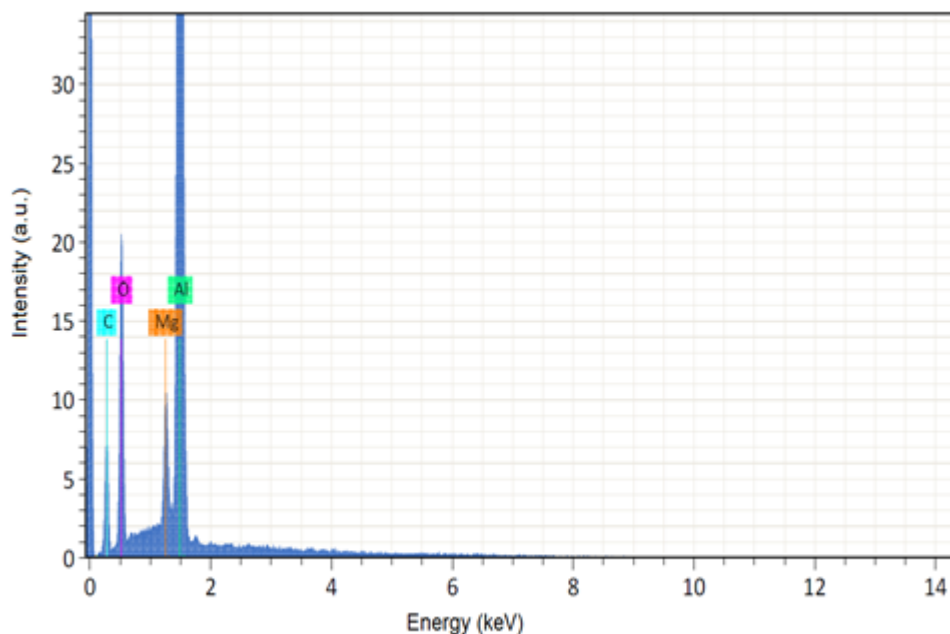
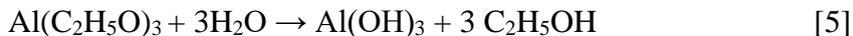


Figure 7. EDS micro chemical analysis of corrosion products found in Al-4Mg-CNT composite corroded in FGE shown in Fig. 6 c).

As mentioned above, corrosion of pure Al can be dissolved in ethanol following a chemical reaction producing an organic compound, aluminum alkoxide,  $\text{Al}(\text{C}_2\text{H}_5\text{O})_3$ , which dissolves in the electrolyte, leaving the metal unprotected [26-28]. These corrosion products, i.e.  $\text{Al}(\text{C}_2\text{H}_5\text{O})_3$  can be transformed in to another type of non-protective corrosion product, by reacting with water according to [35]:



The presence of C, O and Al in the chemical analysis shown in Fig. 7 is an evidence of this reaction, so, the corrosion products found in Fig. 6 c are  $\text{Al}(\text{OH})_3$  whereas the presence of Mg is evidence of reaction [3] above where Mg is dissolved with the release of OH ions increasing the solution pH. Formation of protective  $\text{Al}(\text{OH})_3$  will depend upon the testing temperature, but it has been reported that at 60°C, it will take around 5 hours, and, thus, for a continuous protective, passive  $\text{Al}(\text{OH})_3$  to be formed [26]. This is because before the formation of this film, different stages have to be established, i.e. the formation of an amorphous film during the first hours of immersion, the transformation of this amorphous film in to a crystalline  $\text{AlOOH}$ , and, finally, the formation of the final  $\text{Al}(\text{OH})_3$  [27, 28]. At room temperature, i.e. the one used in this work, the ions mobility and reactivity are not high enough for these reactions to take place and, instead, it will take a much longer time to be formed as a continuous film in the whole metal surface, and, instead, it is formed in very localized places, as shown in Fig. 6 c. Therefore, the metals surface is not completely protected by this  $\text{Al}(\text{OH})_3$  film, and they will undergo a rapid corrosion rate.

#### 4. CONCLUSIONS

The effect of the addition of Mg and CNTs as a reinforcement on the corrosion behavior of mechanically alloyed Al-base composites in in FGE has been evaluated. Polarization curves have shown that there was no evidence of the formation of a passive layer regardless of the Mg contents or the addition of CNTs. The corrosion rate increased with the increase in the Mg contents and with the addition of the CNTs. Specimens exhibited a localized type of corrosion similar to pits. The number of pits increased in number and depth with an increase in the Mg contents, and in size with the addition of CNTs. Results have been explained in terms of micro galvanic cells between CNTs and Fe particles left during its synthesis and the Al-matrix.

#### References

1. S.K. Hoekman, *Renew Energy*, 34(2009) 14.
2. R.C. Costa and J.R. Sodr e, *Fuel*, 89 (2010) 287.
3. F. Nadim, P. Zack, G.E. Hoag and S. Liu, *Energy Policy*, 29 (2001) 1.
4. T.L. Winnington and K.M. Siddiqui, *Automot. Eng.*, 8 (1983) 12.
5. B.D. Jacobucci and R. Schnepf, CRS report for Congress (US): Congressional Research Service, 2008. Report No.: RL34265.
6. E.W. Menezes, R. Catalu a, D. Samios and R. Silva, *Fuel*, 85 (2006) 2567
7. A. Szklo, R. Schaeffer and F. Delgado, *Energy Policy*, 35 (2007) 5411.

8. R.B.C. Cayless, In: Metals handbook. Properties and selection: nonferrous alloys and special-purpose materials, vol. 2. Ohio: ASM International; 1990, 15.
9. F. Bellucci, G. Capobianco, G. Faita and C.A. Farina, *Corros. Sci.*, 28 (1988) 371.
10. G.M. Pinto, J. Nayak and A.N. Shett, *Int. J. Electrochem. Sci.*, 4 (2009)1452.
11. G.B.V. Kumar, C.S.P. Rao, N. Selvaraj and M.S. Bhagyashekar, *J. Miner. Mat. Charac. Eng.*, 9 (2010) 43.
12. J. Safari, G.H. Akbari, A. Shahbazkhan and M.D.Chermahini, *J. Alloys Compd.*, 509 (2011) 9419.
13. X Yao, Y.F. Zheng, J.M. Liang and D.L. Zhang, *Mater. Sci. Eng. A*, 648 (2015) 225.
14. A. Javdani, V. Pouyafar, A. Ameli and A.A. Volinsky, *Mater. Design*, 109 (2016) 57.
15. S.D. Saravanan and M.S. Kumar, *Procedia Eng.*, 64 (2013) 1505.
16. M. Cabeza, I. Feijoo, P. Merino, G. Pena and M.C .Pérez, *Powder Technol.*, 321 (2017) 31.
17. Sheng-Ming Zhou, Xiao-Bin Zhang and Zhi-Peng Ding, *Composites A*, 38 (2007) 301.
18. R. Bradbury Christopher, Jaana-Kateriina Gomon, Kollo Lauri and Kwon Hansang, *J. Alloy Compd.*, 585 (2014) 362.
19. K. Morsi, A.M.K. Esawi and S. Lanka, *Composites A*, 41 (2010) 322.
20. A.M.K. Esawi, K. Morsi and A. Sayed, *Compost. Sci. Technol.*, 70 (2010) 2237.
21. A.M.K. Kesawi and P., *Mat. Sci. Eng. A*, 527 (2010) 5686.
22. B. Wielage and A. Dorner, *Compost. Sci. Tech.*, 59 (1999) 1239.
23. Alaneme Kenneth Kanayo and Olubambi Peter Apata, *J. Mater. Res. Technol.*, 2 (2013)188.
24. Robert Ireland, Luciana Arronche and Valeria La Saponara, *Composites B*, 43 (2012) 183.
25. D. Mendoza-Cachú, C. Mercado-Zúñiga and G. Rosas, *Advances in Condensed Matter Physics 2017*; Volume 2017, Article ID 1751768, 7 pages
26. Y.H. Yoo, I.J. Park and J.G. Kim, *Fuel*, 90 (2011) 1208.
27. I.J. Park, Y.H. Yoo, J.G. Kim, D.H. Kwak and W.S. Ji, *Fuel*, 90 (2011) 633.
28. L.M. Baena, M. Gomez and J.A. Calderon, *Fuel*, 95 (2012) 320.
29. Fukuda Hiroyuki, Szpunar Jerzy and Kondoh Katsuyoshi, *Corros. Sci.*, 52 (2010) 3917.
30. Aung Naing Naing, Zhou Wei and Goh Chwee Sim, *Corros. Sci.*, 52 (2010) 1551.
31. R. Solmaz, G. Kardas and M. Culha, *Electrochim. Acta*, 53 (2008) 5941.
32. T.M. Letcher, C. Heyward, S. Wootton and B. Shuttleworth, *Fuel*, 65 (1986) 891.
33. R. French and P. Malone, *Fluid Phase Equilib*, 228 (2005) 27.
34. N. Marinov, *Int. J. Chem. Kinet.*, 31 (1999) 183.
35. M. Scholz and J. Ellermeier, *Mat -wiss U Werkstofftech*, 37 (2006) 842.